Original Article

# First-in-Man Analysis of the Relationship Between Electrical Rotors From Noninvasive Panoramic Mapping and Atrial Fibrosis From Magnetic Resonance Imaging in Patients With Persistent Atrial Fibrillation

Christian Sohns, MD*; Christine Lemes, MD*; Andreas Metzner, MD; Thomas Fink, MD; Mikhail Chmelevsky, MD; Tilman Maurer, MD; Margarita Budanova, MD; Vladislav Solntsev, PhD; Walther H.W. Schulze, PhD; Wieland Staab, MD; Shibu Mathew, MD; Christian Heeger, MD; Bruno Reißmann, MD; Eugene Kholmovski, PhD; Dietmar Kivelitz, MD; Feifan Ouyang, MD; Karl-Heinz Kuck, MD

***Background***—Late gadolinium enhancement (LGE) cardiovascular magnetic resonance (CMR) imaging can be used to evaluate characteristics of atrial fibrosis. The novel noninvasive epicardial and endocardial electrophysiology system (NEEES) allows for the identification of sources with rotor activity. This study describes a new technique to examine the relationship between rotors and LGE signal intensity in patients with persistent atrial fibrillation (PERS) scheduled for ablation.

***Methods and Results***—Ten consecutive patients underwent pulmonary vein isolation for persistent atrial fibrillation. LGE CMR of both atria was performed, and NEEES-based analysis was conducted to identify rotors. For each mapping point, the intracardiac locations were transferred onto an individual CMR-derived 3-dimensional shell. This allowed the LGE signal intensity to be projected onto the anatomy from the NEEES analysis. NEEES analysis identified a total number of 410 electric rotors, 47.8% were located in the left atrium and 52.2% in the right atrium. Magnetic resonance imaging analysis was performed from 10 right atria and 10 left atria data sets, including 86 axial LGE CMR planes per atrium. The mean LGE burden for left atrium and right atrium was 23.9±1.6% and 15.9±1.8%, respectively. Statistical analysis demonstrated a lack of regional association between the extent of LGE signal intensity and the presence of rotors.

***Conclusions***—This is the first study demonstrating that the presence of rotors based on NEEES analysis is not directly associated with the extent and anatomic location of LGE signal intensity from CMR. Further studies evaluating the relationship between rotors and fibrosis in patients with persistent atrial fibrillation are mandatory and may inform strategies to improve ablation outcome. **(*Circ Arrhythm Electrophysiol*. 2017;10:e004419. DOI: 10.1161/CIRCEP.116.004419.)**

**Key Words:** atrial fibrillation ■ electrophysiology ■ fibrosis ■ gadolinium ■ magnetic resonance imaging



Catheter ablation for persistent atrial fibrillation (PERS) is challenging and associated with only moderate outcome.[1–3] The mechanisms initiating and perpetuating atrial fibrillation (AF) are still not completely understood, and, therefore, ablation strategies are heterogeneous.[1–4] Novel pathophysiological findings, mapping systems, and ablation strategies are currently under investigation and may improve clinical outcomes in chronic forms of AF.

As a potential new approach to improve understanding of the underlying substrate, the translation of phase mapping into clinical applications is promising.[5,6] In parallel, recent progress in numerically solving the inverse problem of electrocardiography opened ways for noninvasive electrocardiography imaging. On the basis of body surface ECG mapping, the electrocardiography imaging allows for the reconstruction of unipolar electrograms and promising results of noninvasive mapping in AF were reported recently.[7] On the basis of this technology, electric rotors and focal sources were demonstrated in patients with PERS.[8–10] In this context, a novel noninvasive epicardial and endocardial electrophysiology system (NEEES) allows for reproducible identification of ectopic electric sources and activity.[11]

Atrial remodeling, including fibrosis and scar, is suggested to play an important role for a potential anchor point of anatomic reentrant circuits.[12,13] Late gadolinium enhancement

Received June 12, 2016; accepted June 29, 2017.

From the Department of Cardiology (C.S., C.L., A.M., T.F., T.M., S.M., C.H., B.R., F.O., K.-H.K.) and Department of Radiology (D.K.), Asklepios Klinik St. Georg, Hamburg, Germany; Department of Cardiac Electrophysiology (M.C., M.B.) and Department of Biostatistics (V.S.), Federal Almazov North-West Medical Research Centre, St-Petersburg, Russia; EP Solutions SA, Yverdon-les-Bains, Switzerland (M.C., W.H.W.S.); Department of Diagnostic and Interventional Radiology, University Medical Center Goettingen, Germany (W.S.); and Comprehensive Arrhythmia Research and Management Center, Salt Lake City, UT (E.K.).

*Drs Sohns and Lemes contributed equally to this work.

Correspondence to Christian Sohns, MD, Department of Cardiology, Asklepios Klinik St. Georg, Lohmühlenstraße 5, 20099 Hamburg, Germany. E-mail c.sohns@asklepios.com



*Circ Arrhythm Electrophysiol* **is available at http://circep.ahajournals.org** **DOI: 10.1161/CIRCEP.116.004419**

### WHAT IS KNOWN

- Late gadolinium enhancement cardiovascular magnetic resonance imaging can be used to evaluate characteristics of atrial fibrosis.
- Sources with electric rotor activity in atrial fibrillation can be identified from noninvasive panoramic mapping.

### WHAT THE STUDY ADDS

- The novel noninvasive epicardial and endocardial electrophysiology system allows for identification of sources with rotor activity in atrial fibrillation.
- The overall distribution of electric rotor activity seems to be individual, whereas we observed a good interindividual correlation for the presence of atrial fibrosis.
- The presence of atrial rotors based on noninvasive epicardial and endocardial electrophysiology system analysis is not directly associated with the extent and anatomic location of late gadolinium enhancement signal intensity from cardiovascular magnetic resonance imaging.

(LGE) cardiovascular magnetic resonance (CMR) imaging can be used to evaluate characteristics of atrial wall abnormalities[14] and might therefore assist in detecting specific area with fibrotic tissue as a substrate for rotor clustering.

In this study, we sought to examine the regional relationship between electric rotors from NEEES and LGE signal intensity (SI) from CMR in patients with PERS scheduled for catheter ablation.

## Methods

Ten consecutive patients with drug-refractory, symptomatic PERS were scheduled to undergo catheter ablation, and all clinical, imaging, and procedural data were recorded. All patients underwent LGE CMR followed by rotor mapping using NEEES in AF the day before ablation. Written informed consent was obtained from each patient before the procedures, and the study was approved by the institutional review board.

### CMR Acquisition

All patients underwent CMR according to our standard protocol.[15] In brief, MRI was performed in a 1.5-T scanner (Magnetom Avanto, Siemens, Germany), using standard body and spine surface coils. To visualize LGE SI, a 3-dimensional (3D) ECG-triggered, inversion recovery prepared turbo gradient echo sequence with respiratory navigator gating was performed. Typical other scan parameters for LGE of the atria were axial imaging volume with a field of view: 360×360×110 mm, voxel size 1.3×1.3×2.5 $mm^3$, repetition time=5.2 ms, echo time=2.4 ms, flip angle of 20°. Depending on patient's respiration, typical scan time for the LGE imaging was 6 to 12 minutes. Data were acquired at mid-diastole, with a 150 ms acquisition window and a low–high k-space ordering, as well as spatial presaturation with inversion recovery fat suppression. The inversion recovery delay time for LGE imaging was determined from an inversion time (TI) scout sequence and was set at a TI value intermediate between the optimal TI values to null myocardium and blood. Previous work has validated this method for reproducible visualization of the late enhancement signal from necrotic tissue.[16] LGE scans were performed 15 minutes after contrast agent administration (0.2 mmol/kg gadoteric acid; Dotarem, Guerbet, France). The number of slices was set for complete atrial coverage (44 slices).

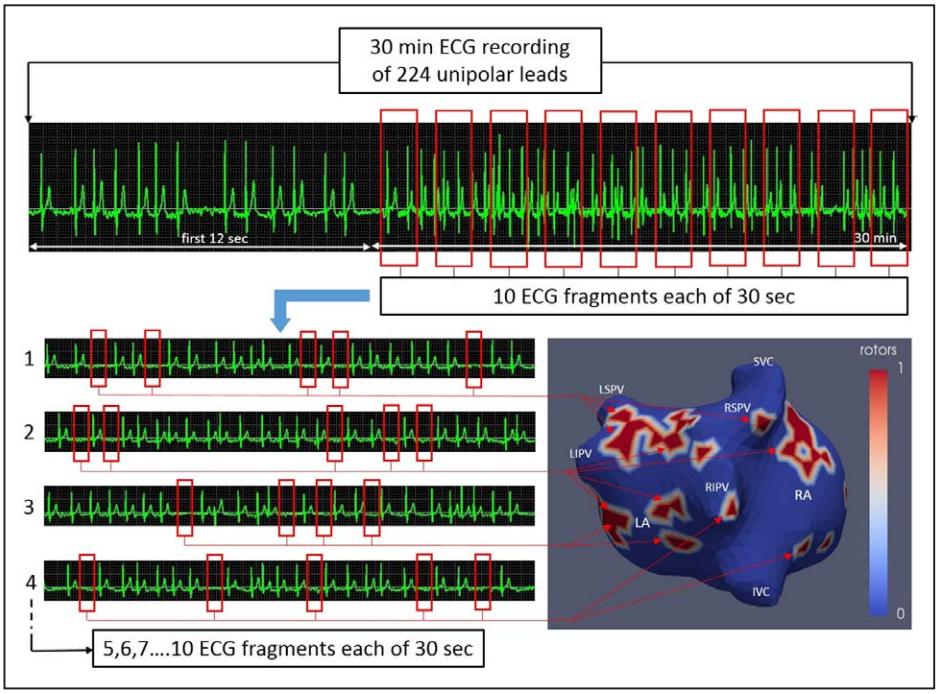


**Figure 1.** Identification of electric rotors in atrial fibrillation (AF) from noninvasive panoramic mapping. Continuous ECGs were recorded for 30 min. Afterward, 10 ECG fragments of 30 s each, with 800 to 1000 ms pauses between adjacent QRS complexes (interval T-Q), were selected for each patient. Each T-Q segment with the length >800 ms was processed to find rotor activity during AF. Sites with rotations on the phase map around stable pivot points were considered as a rotor. Each location of rotor activity was marked and registered onto the reconstructed 3-dimensional atrial model.

## CMR Image Processing

CMR images were processed as described previously.[15–18] In brief, an automatic 3D segmentation of the RA and LA was created from the balanced steady-state–free precession whole-heart acquisition. The LGE acquisition was registered to the 3D balanced steady-state–free precession acquisition and projected on to the 3D shell using a maximum intensity projection technique, whereby the maximum SI within 3 mm of the 3D surface was selected. SIs were then displayed on the 3D RA and LA shells as a number of SDs from the mean SI of the LA blood pool to avoid the need for thresholding. Importantly, this methodology has been previously reported and validated for atrial fibrosis and scar quantification from LGE CMR images.[17–19]

## Noninvasive Epicardial and Endocardial Electrophysiological Mapping

The methodology of electrocardiography imaging with the NEEES system has been reported previously.[20] The Amycard 01C EP laboratory (EP Solutions SA, Yverdon-les-Bains, Switzerland) was used for noninvasive ECG imaging. A total of 224 MRI-compatible body surface mapping electrodes were applied on the patient's torso and connected to the multichannel ECG amplifier (EP Solutions SA). To proof for rotor stability over time, continuous ECGs were recorded for 30 minutes applying a bandwidth of 0.05 to 500 Hz, a sampling rate of 1000 samples/s, and an optional notch filter of 50 Hz (Figure 1). Afterward, the obtained data from CMR were imported into Amycard 01C EP system software in DICOM (Digital Imaging and Communications in Medicine) format to reconstruct a 3D model of the torso and heart. Epicardial atrial 3D models were obtained in high resolution by segmentation and polygonal mesh reconstruction. Furthermore, epicardial unipolar electrograms and phase maps were reconstructed by NEEES inverse problem solution software (EP Solutions SA).

## Noninvasive Identification of Rotors in PERS

Ten ECG fragments of 30 s each, with 800 to 1000 ms pauses between adjacent QRS complexes (interval T-Q), were selected and exported into the Amycard 01C EP laboratory software for each patient. Global bandpass filtration from 3 to 9 Hz was used before phase calculation. Each T-Q segment with the length >800 ms was processed to find rotor activity during AF. Sites with rotations on the phase map around stable pivot points were considered as a rotor. Stable rotor criteria were defined as phase front rotation of at least 360° and rotor core meandering area not exceeding 20 mm along the atrial surface during 1 rotation cycle. Each location of rotor activity was marked and registered onto the reconstructed 3D atrial model (Figure 1). For this purpose, and to compare with LGE data, the LA and RA were systematically divided into segments as demonstrated in Figure 2.

## Comparison of LGE and Rotor Location

Rotor and LGE maps were created from the same CMR data and imported into software custom written with Python (Python Software Foundation). The 2 maps (Figure 3A and 3B) were fused using the iterative closest point algorithm,[21] which computes an optimal affine-based registration for fusion of 2 surfaces.[22] Rotor information could thus be directly analyzed with LGE data as every vertex on the fused shell had an associated rotor and LGE label (Figure 3D). After fusion of the rotor and LGE maps, both quantitative and qualitative comparisons were performed. For each fusion, the registration error was calculated as the mean distance from each vertex on the rotor shell to the nearest vertex on the registered LGE shell (Figure 4), and a map of absolute distances between the fused models was created (Figure 3C). For further analysis, the rotor and LGE maps were visualized using Paraview (Kitware Inc) and analyzed based on the anatomic segments.

## Statistical Analysis

The preliminary exploratory analysis was conducted to evaluate the distribution of different data; an initially $P$ value <0.05 was considered as statistically significant. Patient clinical characteristics and spatial anatomic distribution of rotors and LGE SI data were reported using descriptive statistics. The amount of rotor data for each atrial segment was not normally distributed, whereas LGE data did not severely differ from normal distribution. On the basis of these findings, continuous variables are expressed as median with min/max range or 25% to 75% interquartile range for patient clinical characteristics and rotor spatial distribution and as mean and SD for the LGE data. Categorical data are presented as numbers and percentages. The Pearson $\chi^2$ and Fisher exact tests were used for the analysis of cross tabulation tables of categorical data for clinical parameters. The Mann–Whitney $U$ test was performed to compare independent samples, including patients' characteristics with LGE SI and rotor distribution. These tests were used as exploratory analysis tools.

The Spearman rank correlation was calculated to compare the continuous variables of LGE data and rotors. The Wilcoxon signed-rank test was performed to compare 2 continuous variables by means of LGE SI and mean values of rotors in the RA and LA. Furthermore, Friedman 1-way ANOVA by ranks test was used to compare multiple continuous variables of LGE SI and rotor values for all atrial segments. After that, we performed joining cluster analysis (Ward method, 1-Pearson $r$ criterion) of LGE data and rotor distribution among all patients. All comparisons were made in accordance with cross-sectional study design. Finally, a $P$ value <0.01 was considered as statistically significant because of the Bonferroni correction and relatively small number of analyzed patients. Comprehensive statistical analysis was performed using Statistica v.10 (Statsoft Inc) and SPSS v.23 (IBM Corp).

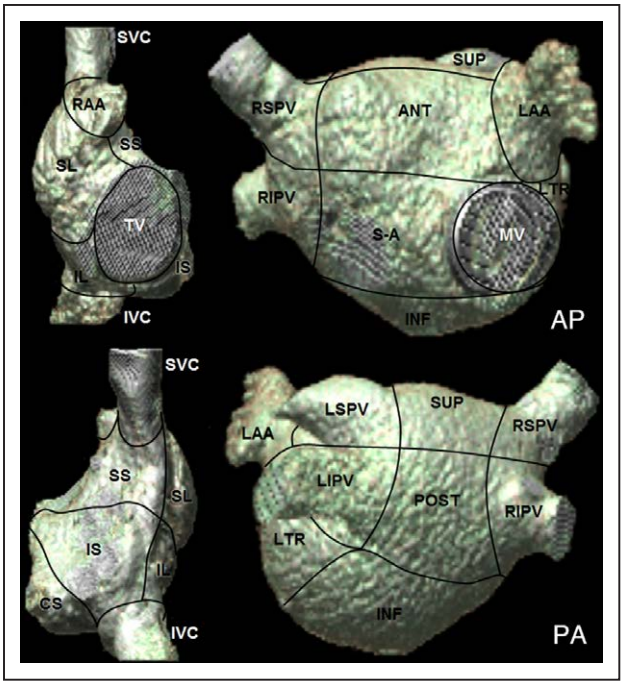


**Figure 2.** Three-dimensional reconstruction from preprocedural cardiovascular magnetic resonance imaging of the right (RA) and left atrium (LA) in anterior/posterior (AP) and posterior/anterior (PA) view. The RA was divided into the following segments: right atrial appendage (RA RAA), coronary sinus ostial area (RA CS), superior lateral (RA SUP LAT), inferior lateral (RA INF LAT), superior septal (RA SUP SEP), inferior septal (RA INF SEP), superior cava vein (SCV), and inferior cava vein (ICV). The LA was divided into the following segments: superior (LA SUP), posterior (LA POST), anterior (LA ANT), inferior (LA INF), lateral (LA LAT), right superior pulmonary vein (LA RSPV), right inferior PV (LA RIPV), left superior PV (LA LSPV), left inferior PV (LA IPV), septal-anterior (LA SEPT ANT), and left atrial appendage (LAA).

# Results

## Clinical Characteristics

Ten patients (median age 67 years; range 46–77 years, 5 male) with PERS underwent LGE CMR followed by rotor

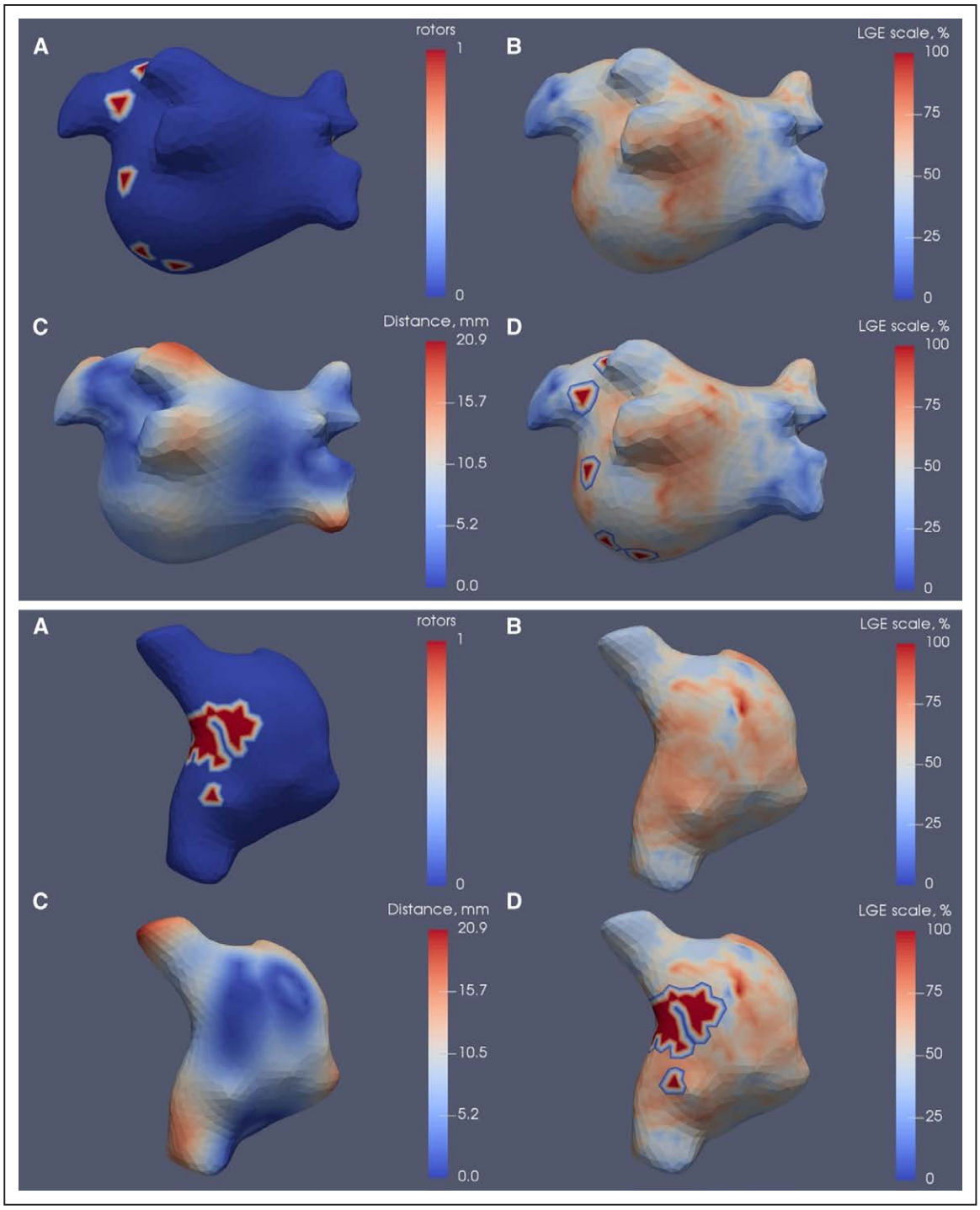


**Figure 3.** Patient-specific example for image processing, reconstruction of the individual rotor location and extent of atrial fibrosis, and fusion of the models for final analysis. **Upper**, **A**, Reconstrution of the left atrium (LA) with anatomic distribution of rotors from noninvasive epicardial and endocardial electrophysiology system (NEEES). **B**, Individual 3-dimensional model of the LA demonstrating the level of late gadolinium enhancement (LGE) signal intensity (SI). **C**, Fusion of the models and visualization of the absolute distances between fused models. **D**, Merge of the individual rotor (**A**) and LGE SI reconstruction (**B**) for further analysis. **Lower**, **A**, Reconstrution of the right atrium (RA) with anatomic location of rotors from NEEES. **B**, Individual 3-dimensional model of the RA demonstrating the level of LGE SI. **C**, Fusion of the models and visualization of the absolute distances between fused models. **D**, Merge of the individual rotor (**A**) and LGE SI reconstruction (**B**) for further analysis.

analysis using NEEES. Median AF duration per patient was 8 months (range 1–45); none of the patients underwent previous ablation. In all patients at least 1 antiarrhythmic drug failed prior the indication to undergo catheter ablation. The clinical baseline characteristics of the entire study population are depicted in Table 1. There was no significant association between clinical characteristics and the amount of LGE SI or anatomic localization of rotors.

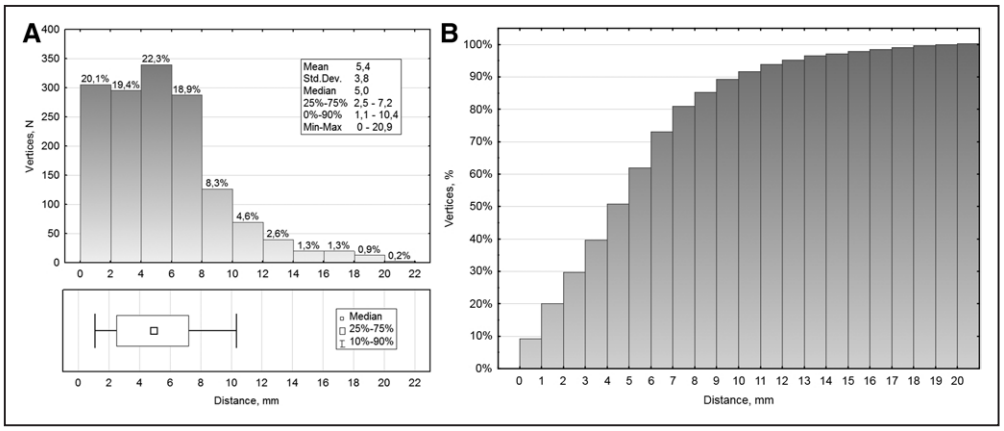


**Figure 4.** Demonstration of the accuracy of the fused atrial models. The registration error for each fusion was calculated as the mean distance between the models. **A**, Histogram with mean (SD) and box-and-whisker plot for median and interquartile range (IQR) of the absolute distances between the models. **B**, Cumulative histogram of the mean distances between the fused models. This histogram demonstrates the cumulative percent of vertices (*y* axis) against the specified distance (*x* axis).

## Rotor Analysis and Location

In all 10 patients, a total number of 410 rotors were identified from NEEES, with 196 (47.8%) occurring in the LA and 214 (52.2%) in the RA. Mean value of total observation time for NEEES was 18.9 s; mean (SD) value of ECG fragment length was 561 ms (154 ms). The median (interquartile range, 25%–75%) number of revealed rotors per patient was n=20 (14–30), n=20 (11–22), and n=44 (24–56) for the RA, LA, and total, respectively. The majority of the rotors in the LA was located along the inferior wall n=66 (minimal 1–17 maximal rotor(s) at this location) and in vicinity to the right superior pulmonary vein (PV) n=35 (0–10). RA sources were predominantly detected in the superior lateral segment n=84 (0–18). Anatomic distribution of rotors and rotor occurrence rate were completely different in the RA, LA, and between all segments ($P$<0.001). There was no significant difference between mean number of rotors for the RA and LA ($P$=0.72). Table 2 shows the whole distribution of right- and left-sided rotors and the total number of rotors per patient. Rotors were not sustained and showed meandering rotor activity with their core traveling over an area of >2 cm$^2$. Yet, the occurrence of rotational activity demonstrated a stochastic pattern with clustering in regions specific for each individual. In consequence, a rotor location could not be observed at a certain site but more broadly as region or anatomic segment. In this context, Figure 5A demonstrates the rotor distribution in both atria per segment. In addition, the interindividual distribution of rotors was also totally different as demonstrated in Figure 6 ($P$=0.006).

**Table 1. Baseline Patient Characteristics**

| Characteristic | Value |
|---|---|
| Age, y | 67 (46–77) |
| Persistent atrial fibrillation (%) | 10 (100) |
| Duration of atrial fibrillation, mo | 8 (1–178) |
| Left atrial diameter, mm | 48 (37–60) |
| Left ventricular ejection fraction (%) | 52 (30–65) |
| Sex: male, n (%) | 5 (50) |
| $CHA_2DS_2$-VASc Score | 3 (0–4) |
| Heart failure (%) | 4 (40) |
| Hypertension (%) | 6 (60) |
| Coronary artery disease (%) | 4 (40) |
| Previous antiarrhythmic drugs (%) | 9 (90) |
| Oral anticoagulation | |
| Warfarin [%] | 3 [30] |
| NOAC [%] | 7 [70] |

Values are expressed as median (min/max) or as N (%). NOAC indicates novel oral anticoagulants.

## Anatomic Distribution of LGE SI

The majority of the LGE SI burden from preprocedural CMR was observed in the LA, predominantly at the posterior wall and along the left atrial appendage. In this context, the total extent of LGE SI was higher when compared with the RA when considering all patients. The mean LGE burden as a percentage of the total LA and RA surface was 23.9±1.6% and 15.9±1.8%, as well as 20.5±1.2% in both atria, respectively. Focusing on the mean LGE burden, we observed a significant difference for the LA and RA ($P$=0.005). In this context, the sectors with the highest amount of LGE SI were located along the posterior wall (40.5±4.4%) and in the left atrial appendage (34.9±6.2%). For the RA, the highest amount of LGE SI was detected in the superior septal (22.6±5.28%) and inferior septal wall (21.2±7.7%), respectively. Table 2 shows the whole distribution of mean LGE SI per patient, as well as the total LGE burden for the RA and LA, whereas Figure 5B demonstrates the distribution of LGE SI per atrial segment for the RA and LA. The interindividual distribution of LGE SIs for all segments irrespective of their anatomic location was completely different among the patients ($P$<0.001). In contrast, the interpatients distribution of the LGE SIs was not significantly different (Figure 6B; $P$=0.056), and a significant correlation was observed for the LGE SI extent when comparing all patients.

**Table 2. Patient-Specific Distribution of LGE SI and Rotors From Noninvasive Epicardial and Endocardial Electrophysiology System**

| Patients | Mean LGE, LA, % (SD) | Mean LGE, RA, % (SD) | Mean LGE, Total, % (SD) | Rotors, LA, % (Fr) | Rotors, RA, % (Fr) | Rotors, Total, N (Fr) |
|---|---|---|---|---|---|---|
| 1 | 22.8 (7.3) | 15.1 (5.5) | 19.5 (7.5) | 29.2 (0.77) | 70.8 (1.87) | 24 (2.65) |
| 2 | 25.0 (10.4) | 15.0 (5.6) | 20.8 (9.9) | 55.0 (1.08) | 45.0 (0.88) | 40 (1.96) |
| 3 | 20.2 (6.9) | 14.9 (3.5) | 17.9 (6.2) | 87.5 (2.30) | 12.5 (0.33) | 24 (2.62) |
| 4 | 23.6 (9.3) | 17.9 (6.9) | 21.2 (8.7) | 44.0 (1.17) | 56.0 (1.49) | 25 (2.66) |
| 5 | 23.1 (8.5) | 18.1 (5.7) | 21.0 (7.7) | 29.3 (0.75) | 70.7 (1.81) | 58 (2.56) |
| 6 | 25.2 (11.6) | 18.2 (7.6) | 22.2 (10.5) | 42.6 (0.90) | 57.4 (1.22) | 47 (2.12) |
| 7 | 25.1 (9.8) | 17.6 (8.2) | 21.9 (9.7) | 33.9 (0.81) | 66.1 (1.58) | 56 (2.38) |
| 8 | 24.2 (8.5) | 15.2 (6.6) | 20.4 (8.8) | 59.3 (1.46) | 40.7 (1.00) | 54 (2.46) |
| 9 | 25.8 (7.2) | 13.2 (3.0) | 20.5 (8.5) | 68.8 (0.44) | 31.3 (0.20) | 16 (0.65) |
| 10 | 24.0 (8.5) | 13.9 (3.8) | 19.7 (8.5) | 54.5 (1.40) | 45.5 (1.17) | 66 (2.57) |

Values are expressed as mean % (SD) for LGE and % of N (Fr) for AF rotors. The interindividual late gadolinium enhancement (LGE) signal intensity (SI) distribution is similar in the left (LA) and in the right atria (RA). In addition, the amount of LGE SI is higher in the LA when compared with the RA. The interindividual distribution of rotors differs in the RA and LA. This is also true for the rotors occurrence (Fr) rate per patient. This leads to the conclusion that the patients with persistent AF and similar clinical characteristics will have almost the same distribution pattern for LGE SI, but different anatomic distribution of rotors.

### Relationship Between Atrial Fibrosis and Rotor Distribution

The distribution of LGE SI and rotors among all patients is demonstrated in Table 2. There was no statistical significant correlation between anatomic rotor location from NEEES and the amount of LGE SI from CMR in the RA and LA, as to be appreciated from the correlation diagram in Figure 7. In addition, NEEES identified the minimal presence of segmental rotor activity (<6% for the LA and <2% for the RA) inside atrial segments with LGE SI >25% (LA) and 20% (RA), respectively (Figure 5).

Despite this fact, we observed a higher interindividual correlation for the presence of LGE SI per segment when compared with the anatomic distribution of rotors. An additional joining cluster analysis using the Ward method (1-Pearson *r* criterion) was performed as demonstrated in Figure 8. The results of this cluster analysis demonstrate a clear structure of clusters where the strongest similarities (short linkage distances) were observed between patients inside the LGE SI group, and the strongest dissimilarities were found between the group of LGE SI and rotors. This finding can be regarded as a lack of direct anatomic association between the extent of LGE SI and presence of rotors in the current patient cohort.

### Fusion Accuracy of the Left and Right Atrial Models

The mean number of vertices per fused atrial model was 1523, and the mean (SD) distance between each LGE SI and rotor model was 5.4±3.8 mm. The absolute values for minimal distance between the fused models were <0.1 mm and 20.9 mm for the maximal distance, whereas the 25% to 75% range was 2.5 to 7.2 mm (Figure 4A). In this context, the cumulative histogram analysis of the mean distances between the fused models shows that 89% of all vertices had distance <10 mm, and even 51% <5 mm (Figure 4B). Furthermore, 11% of the area with distances >10 mm was located in the pulmonary veins and the distal part of the left atrial appendage.

## Discussion

### Main Finding

The main finding of this study was that in patients with PERS, rotors identified applying NEEES have no direct anatomic relationship with regions of elevated LGE SI in the RA and LA. This is the first study to specifically analyze the correlation between rotors in PERS from noninvasive panoramic mapping and the amount of preprocedural atrial fibrosis from CMR.

### Role of NEEES and Invasive Mapping for Rotors in AF

Identification and localization of AF-initiating triggers and AF-maintaining substrate is a prerequisite for effective AF treatment strategies either applying invasive or noninvasive mapping methods. In contrast to body surface mapping, the focal impulse and rotor modulation–guided ablation strategy is an invasive approach. A potential limitation of this system is that stable rotors may be underestimated because of a mismatch of the multipolar basket catheter and the atrial anatomy and thereby a lack of atrial wall-to-tissue contact. Moreover, the multipolar basket catheter cannot cover the total atrial surface of the RA and LA at the same time, which is a pivotal requirement for correct mapping of unstable arrhythmias, such as AF. This could be an explanation why no correlation was found between rotor localization from invasive mapping and complex fractionated atrial electrogram sites[23] and area of low voltage from electroanatomical mapping.[24] In this context, our data from NEEES clearly show that the distribution of rotors demonstrated some common trends. On the one hand, rotors were not sustained and showed meandering rotor activity with their core traveling along the atrial surface. Yet, the occurrence of rotational activity demonstrated a stochastic pattern with clustering in regions specific for every patient. This finding is in line with previous data from Haissaguerre et al[9] also evaluating another panoramic noninvasive atrial mapping system in AF. In particular, in all patients, the majority of identified rotors were observed in the LA inferior wall (20.1%) and RA

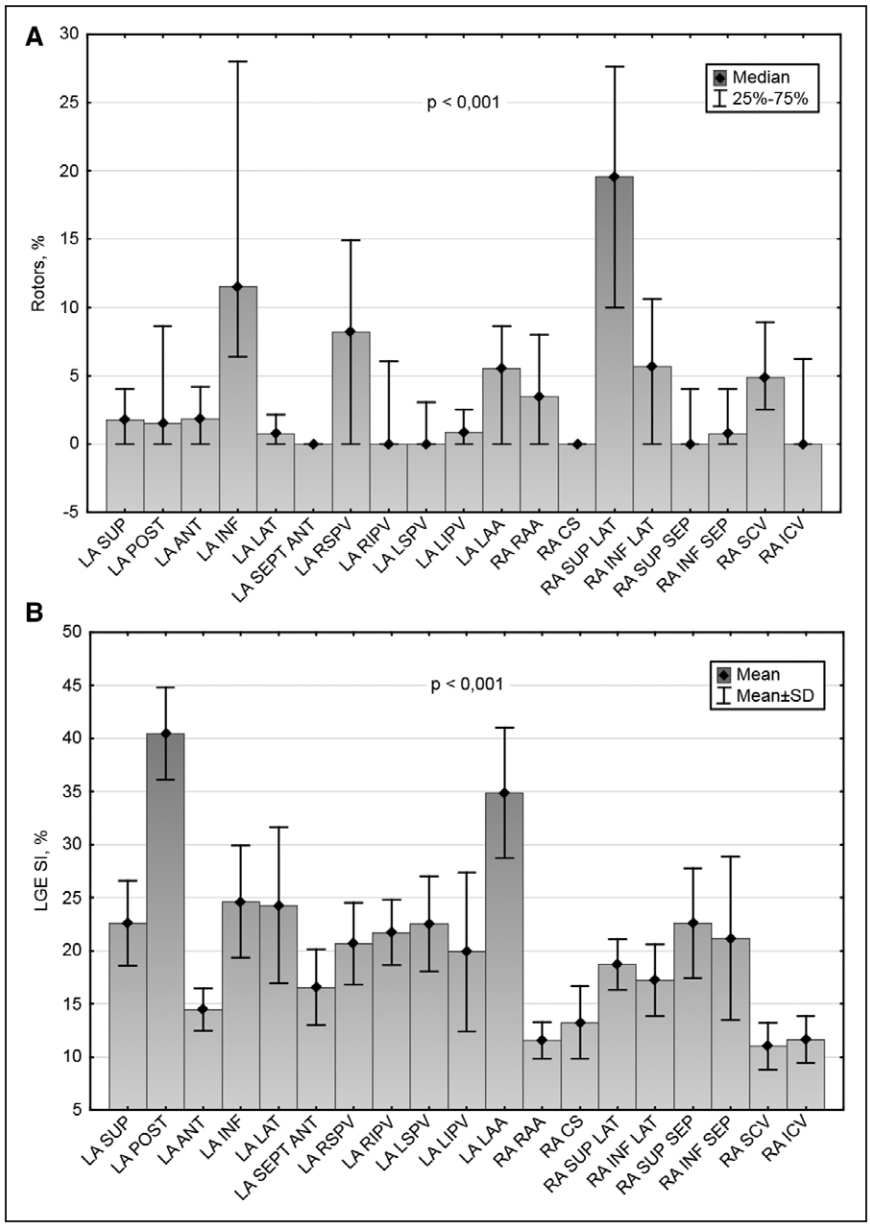


**Figure 5.** **A**, Box-and-whisker plot histogram of the anatomic distribution of rotors from noninvasive epicardial and endocardial electrophysiology system (NEEES) divided per atrial segment. **B**, Box-and-whisker plot histogram of the extent of late gadolinium enhancement (LGE) signal intensity from magnetic resonance imaging per atrial segment. The LA was divided into the following segments: superior (LA SUP), posterior (LA POST), anterior (LA ANT), inferior (LA INF), lateral (LA LAT), right superior pulmonary vein (LA RSPV), right inferior PV (LA RIPV), left superior PV (LA LSPV), left inferior PV (LA IPV), septal-anterior (LA SEPT ANT), and left atrial appendage (LAA). The RA was divided into the following segments: right atrial appendage (RA RAA), coronary sinus ostial area (RA CS), superior lateral (RA SUP LAT), inferior lateral (RA INF LAT), superior septal (RA SUP SEP), inferior septal (RA INF SEP), superior cava vein (SCV), and inferior cava vein (ICV).

superior lateral wall (17.9%), respectively (Table 2; Figure 5). On the other hand, the distribution of the rotors between all segments and among all patients was completely different, and these findings were statistically significant. Thereby, our data demonstrate that the overall spatial distribution of atrial rotors seems to be individual, which may explain the lack of significant interindividual correlation. Furthermore, we observed higher interindividual correlations for the presence of fibrosis when compared with the anatomic distribution of rotors. A potential benefit of NEEES when compared with invasive rotor mapping is the panoramic visualization of rotor activity and therefore a more detailed information about its location and activity with equal spatial resolution for the whole atrial surface. However, the specific anatomic rotor location from NEEES might differ from endocardial rotor mapping, and a direct comparison of invasive and noninvasive rotor mapping approaches is still pending in humans. It has to be taken into consideration that data derived from prospective multicenter studies are necessary before a conclusion with focus on advantages and disadvantages of invasive and noninvasive mapping strategies for rotors in AF can be drawn.

## Relationship Between Atrial Fibrosis and Rotor Distribution

There is evidence from experimental models that structural modalities, such as fibrosis or scar tissue, may be important in anchoring fibrillatory rotors.[13] Furthermore, recent data suggest that stable rotors in AF are located along the border zone between fibrotic and healthy atrial tissue.[25] In this context, CMR allows to distinguish between atrial fibrosis and normal atrial tissue in patients with AF.[13] Also, in virtual studies using in silico CMR-based models of patient-specific LA structure and LGE SI, AF was inducible according to the level of LGE SI.[26] Recently, Chrispin et al[27] reported their data about regional association between atrial LGE SI from CMR and AF rotors from a focal impulse and rotor modulation–guided

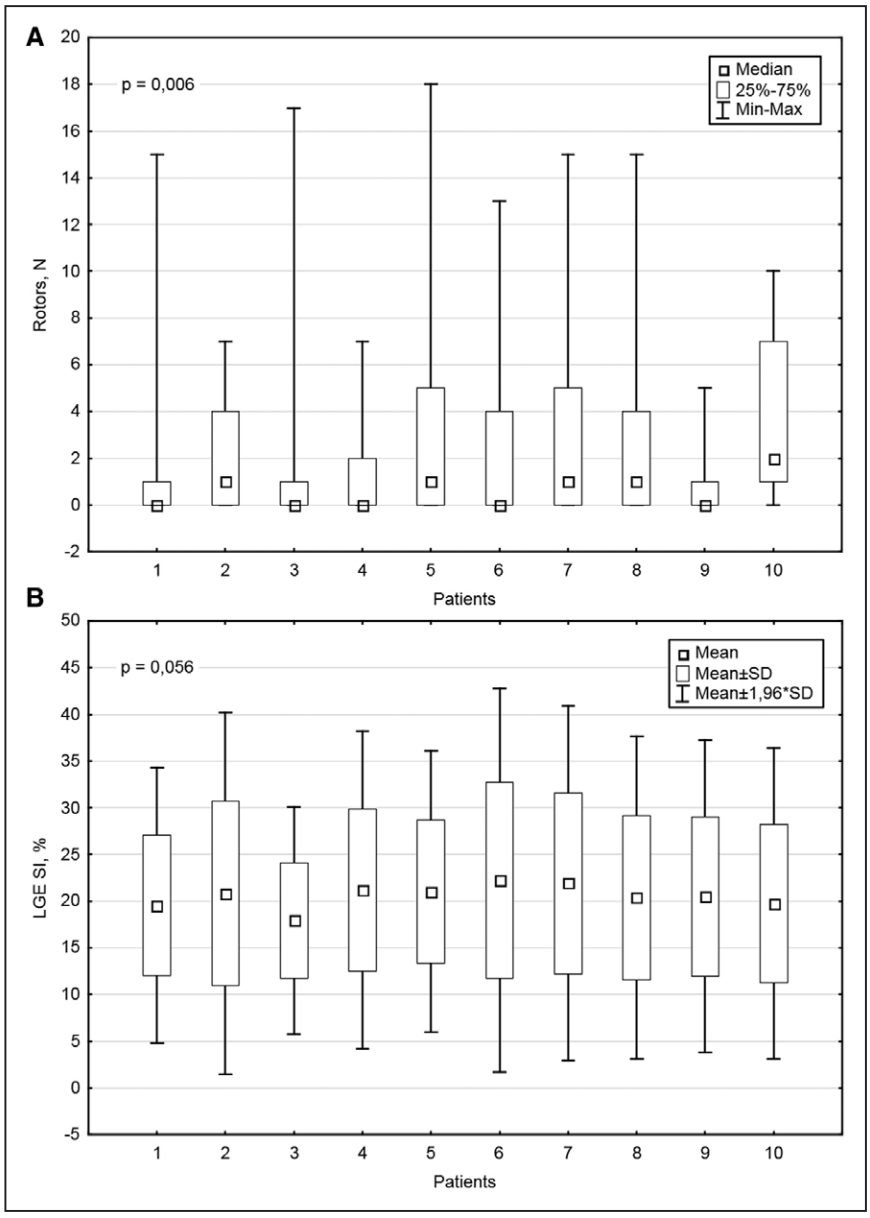


**Figure 6.** **A**, Box-and-whisker plot of the distribution of rotors from noninvasive epicardial and endocardial electrophysiology system (NEEES) for all patients. **B**, Box-and-whisker plot of the distribution of late gadolinium enhancement (LGE) signal intensity (SI) from magnetic resonance imaging for all patients.

mapping approach. The authors found that there was no correlation between the incidence of rotors in PERS from invasive mapping and the global extent of atrial LGE SI.[27] This is in line with our findings as one can see from Figures 6 through 8. NEEES identified a total number of 410 rotors (41 rotors per patient), with 47.8% occurring in the LA and 52.2% in the RA. The mean LGE SI burden was 23.9±1.6% for the LA and 15.9±1.8% for the RA. In concordance with the findings of Chrispin et al,[27] statistical analysis could not detect a significant association between the extent of LGE SI and the presence of rotors in our cohort. This might lead to the suggestion that electroanatomic remodeling in patients with PERS has some different components, which are still not completely understood. On the one hand, our data indicate that fibrosis and scar tissue can be visualized using CMR at typical locations representing an anatomic substrate as a target for catheter ablation, which is in line with previous data.[28,29] On the other hand, NEEES and invasive mapping methods identified the presence of electric rotors without any anatomic reference.[27] This could probably be explained by the fact that rotors move and meander around a core[8,9,13] and might therefore not stay stable at the same position during MRI and NEEES. To finally understand that phenomenon, an analysis of rotor stability over the time and its correlation with LGE SI would be essential.

## Clinical Implication

Strategies to improve the efficacy of catheter ablation in patients with PERS are warranted. New ablation targets include among others complex fractionated atrial electrograms, additional linear lesions sets, homogenization of atrial fibrosis, modulation of the autonomic nervous system, left atrial appendage isolation, and targeting electric rotors from invasive and noninvasive mapping. The initial results of rotor-guided ablation approaches are heterogeneous,[30,31] and the idea to ablate electric rotors needs further validation.[32] In addition, Akoum et al[29,33] recently

| Patients | 01-AFrot | 02-AFrot | 03-AFrot | 04-AFrot | 05-AFrot | 06-AFrot | 07-AFrot | 08-AFrot | 09-AFrot | 10-AFrot |
|---|---|---|---|---|---|---|---|---|---|---|
| 1 | 0,38 | -0,20 | -0,13 | -0,05 | 0,04 | -0,08 | -0,15 | -0,31 | -0,51 | -0,32 |
| 2 | 0,85 | 0,35 | 0,15 | -0,06 | 0,36 | 0,55 | 0,23 | 0,53 | 0,63 | 0,50 |
| 3 | 0,77 | 0,79 | -0,22 | 0,38 | 0,02 | 0,09 | 0,24 | 0,54 | 0,27 | 0,29 |
| 4 | 0,61 | 0,39 | 0,29 | -0,06 | 0,15 | 0,32 | 0,08 | 0,27 | 0,23 | 0,18 |
| 5 | 0,78 | 0,69 | 0,65 | 0,54 | 0,25 | 0,45 | 0,45 | 0,24 | 0,25 | 0,45 |
| 6 | 0,80 | 0,76 | 0,68 | 0,70 | 0,69 | 0,00 | 0,37 | 0,25 | 0,51 | 0,65 |
| 7 | 0,94 | 0,85 | 0,78 | 0,60 | 0,77 | 0,84 | 0,02 | 0,46 | 0,38 | 0,74 |
| 8 | 0,78 | 0,69 | 0,70 | 0,53 | 0,68 | 0,55 | 0,72 | 0,10 | 0,47 | 0,54 |
| 9 | 0,64 | 0,68 | 0,73 | 0,35 | 0,52 | 0,35 | 0,60 | 0,82 | 0,08 | 0,63 |
| 10 | 0,52 | 0,44 | 0,32 | 0,73 | 0,34 | 0,39 | 0,44 | 0,64 | 0,71 | -0,18 |
| | 01-LGE | 02-LGE | 03-LGE | 04-LGE | 05-LGE | 06-LGE | 07-LGE | 08-LGE | 09-LGE | 10-LGE |

*Color map of correlation (r)*

r > 0,7
0,5 <r< 0,7
0,2 <r< 0,5
r < 0,2

**Figure 7.** Correlation diagram (Correlogram) of rotors from noninvasive epicardial and endocardial electrophysiology system (NEEES) and late gadolinium enhancement (LGE) signal intensity (SI) per patient. The table demonstrates the Spearman rank correlation coefficients between rotors and LGE SI for each patient. The table cells are colored according to the magnitude of the correlation, ranging from red for high-level degree of correlation to gray for low-level or negative correlation. The variables are sorted; thus, LGE data are distributed in the left bottom triangle and rotor data—in the right upper triangle of the table. The correlogram shows that there was no significant correlation between rotor location and LGE SI burden per patient. The table demonstrates a high interindividual correlation for the extent of LGE SI, as well as a low correlation for the rotors. Red colored numbers inside the cell stay for a significant correlation ($P$<0.01). White color cells show the correlation between LGE SI and rotors per patient.

reported their interesting ablation approach to target preprocedural fibrosis in patients with PERS. However, currently, we have to conclude that fibrosis from CMR cannot predict the presence of electric rotors based on standard anatomic segmentation, and further data are necessary to determine whether a rotor-based ablation strategy alone or a combination with another ablation target may have the potential to improve the outcomes after ablation for PERS.

## Study Limitations

This is not an outcome-based study. It seeks to demonstrate a new method applying CMR to quantify the correlation

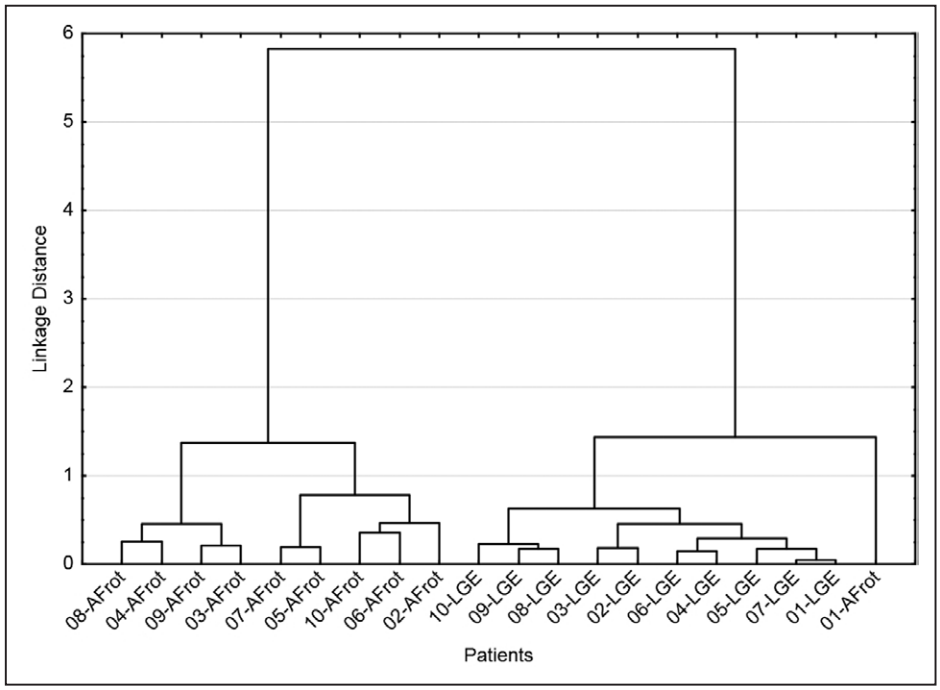


**Figure 8.** Hierarchical tree diagram (joining cluster analysis) for segmental rotor distribution and late gadolinium enhancement (LGE) signal intensity (SI) burden using the Ward method (1-Pearson *r* criterion). Linkage distance shows the level of similarity between all analyzed groups in a full data set. Sorting out the data for the groups was performed in a way that the degree of association between the objects is best if they were grouped close together by having nearly a total correlation. Thus, the lower the level of aggregation (shortest linkage distance), the closer are observed groups, and, therefore, the more similar are the initial objects in the full data set.

between LGE SI and the presence of rotors from noninvasive mapping in patients with PERS before catheter ablation. Therefore, the patient numbers are small, and a follow-up of the ablation outcome was not assessed. One very useful outcome of the study is the lack of direct anatomic correlation between the extent of LGE SI and rotors from NEEES-based segmentation, demonstrating that LGE SI could not be used as a surrogate parameter for the presence of electric rotors. However, it has to be considered that the specific algorithm for the NEEES-based rotor distribution might differ from endocardial rotor mapping findings, and a direct comparison of invasive and noninvasive rotor mapping approaches has not yet been performed in vivo. In addition, the software used for the analysis of atrial fibrosis does not differentiate between preablation fibrosis and atrial ablation-induced scar tissue. In this context, a recent study by Karim et al[19] found no significant differences with focus on segmentation of scar tissue from LGE CMR of the LA comparing different algorithms. The segmentation software used in this study has been described previously and can be considered as reproducible.[15–18] It remains questionable whether this is also true for the analysis of preablation scar formation. However, we cannot completely exclude that another algorithm for segmentation of atrial scar tissue from LGE CMR might result in different results, especially when using a software that allows for differentiation of fibrosis and ablation-induced scar tissue.

## Conclusions

There is no direct anatomic relationship between the amount and location of RA and LA LGE SI and the presence of electric rotors identified from NEEES. Further prospective studies are necessary to determine whether the amount of LGE SI is associated with rotor activity before final conclusions can be drawn.

## Acknowledgments

We greatly appreciate the help of Maria Chaykovskaya (EP Solutions SA, Yverdon-les-Bains, Switzerland) with the segmentation of atrial models.

## Disclosures

Drs Chmelevsky and Schulze are consultants of EP Solutions SA. The other authors report no conflicts.

## References

1. Scherr D, Khairy P, Miyazaki S, Aurillac-Lavignolle V, Pascale P, Wilton SB, Ramoul K, Komatsu Y, Roten L, Jadidi A, Linton N, Pedersen M, Daly M, O'Neill M, Knecht S, Weerasooriya R, Rostock T, Manninger M, Cochet H, Shah AJ, Yeim S, Denis A, Derval N, Hocini M, Sacher F, Haissaguerre M, Jais P. Five-year outcome of catheter ablation of persistent atrial fibrillation using termination of atrial fibrillation as a procedural endpoint. *Circ Arrhythm Electrophysiol*. 2015;8:18–24. doi: 10.1161/CIRCEP.114.001943.
2. Verma A, Jiang CY, Betts TR, Chen J, Deisenhofer I, Mantovan R, Macle L, Morillo CA, Haverkamp W, Weerasooriya R, Albenque JP, Nardi S, Menardi E, Novak P, Sanders P; STAR AF II Investigators. Approaches to catheter ablation for persistent atrial fibrillation. *N Engl J Med*. 2015;372:1812–1822. doi: 10.1056/NEJMoa1408288.
3. Tilz RR, Rillig A, Thum AM, Arya A, Wohlmuth P, Metzner A, Mathew S, Yoshiga Y, Wissner E, Kuck KH, Ouyang F. Catheter ablation of long-standing persistent atrial fibrillation: 5-year outcomes of the Hamburg Sequential Ablation Strategy. *J Am Coll Cardiol*. 2012;60:1921–1929. doi: 10.1016/j.jacc.2012.04.060.
4. Cappato R, Calkins H, Chen SA, Davies W, Iesaka Y, Kalman J, Kim YH, Klein G, Natale A, Packer D, Skanes A, Ambrogi F, Biganzoli E. Updated worldwide survey on the methods, efficacy, and safety of catheter ablation for human atrial fibrillation. *Circ Arrhythm Electrophysiol*. 2010;3:32–38. doi: 10.1161/CIRCEP.109.859116.
5. Nash MP, Mourad A, Clayton RH, Sutton PM, Bradley CP, Hayward M, Paterson DJ, Taggart P. Evidence for multiple mechanisms in human ventricular fibrillation. *Circulation*. 2006;114:536–542. doi: 10.1161/CIRCULATIONAHA.105.602870.
6. Massé S, Downar E, Chauhan V, Sevaptsidis E, Nanthakumar K. Ventricular fibrillation in myopathic human hearts: mechanistic insights from *in vivo* global endocardial and epicardial mapping. *Am J Physiol Heart Circ Physiol*. 2007;292:H2589–H2597. doi: 10.1152/ajpheart.01336.2006.
7. Cuculich PS, Wang Y, Lindsay BD, Faddis MN, Schuessler RB, Damiano RJ Jr, Li L, Rudy Y. Noninvasive characterization of epicardial activation in humans with diverse atrial fibrillation patterns. *Circulation*. 2010;122:1364–1372. doi: 10.1161/CIRCULATIONAHA.110.945709.
8. Haissaguerre M, Hocini M, Shah AJ, Derval N, Sacher F, Jais P, Dubois R. Noninvasive panoramic mapping of human atrial fibrillation mechanisms: a feasibility report. *J Cardiovasc Electrophysiol*. 2013;24:711–717. doi: 10.1111/jce.12075.
9. Haissaguerre M, Hocini M, Denis A, Shah AJ, Komatsu Y, Yamashita S, Daly M, Amraoui S, Zellerhoff S, Picat MQ, Quotb A, Jesel L, Lim H, Ploux S, Bordachar P, Attuel G, Meillet V, Ritter P, Derval N, Sacher F, Bernus O, Cochet H, Jais P, Dubois R. Driver domains in persistent atrial fibrillation. *Circulation*. 2014;130:530–538. doi: 10.1161/CIRCULATIONAHA.113.005421.
10. Lim HS, Zellerhoff S, Derval N, Denis A, Yamashita S, Berte B, Mahida S, Hooks D, Aljefairi N, Shah AJ, Sacher F, Hocini M, Jais P, Haissaguerre M. Noninvasive mapping to guide atrial fibrillation ablation. *Card Electrophysiol Clin*. 2015;7:89–98. doi: 10.1016/j.ccep.2014.11.004.
11. Wissner E, Revishvili A, Andreas A, Tsyganov A, Kalinin V, Lemes C, Saguner AM, Maurer T, Sebastian D, Sopov O, Labarkava E, Chmelevsky M, Kuck KH. Noninvasive epicardial and endocardial mapping of premature ventricular contractions. *Europace*. 2017;19:843–849. doi: 10.1093/europace/euw103.
12. Ashihara T, Haraguchi R, Nakazawa K, Namba T, Ikeda T, Nakazawa Y, Ozawa T, Ito M, Horie M, Trayanova NA. The role of fibroblasts in complex fractionated electrograms during persistent/permanent atrial fibrillation: implications for electrogram-based catheter ablation. *Circ Res*. 2012;110:275–284. doi: 10.1161/CIRCRESAHA.111.255026.
13. Gonzales MJ, Vincent KP, Rappel WJ, Narayan SM, McCulloch AD. Structural contributions to fibrillatory rotors in a patient-derived computational model of the atria. *Europace*. 2014;16(suppl 4):iv3–iv10.
14. Marrouche NF, Wilber D, Hindricks G, Jais P, Akoum N, Marchlinski F, Kholmovski E, Burgon N, Hu N, Mont L, Deneke T, Duytschaever M, Neumann T, Mansour M, Mahnkopf C, Herweg B, Daoud E, Wissner E, Bansmann P, Brachmann J. Association of atrial tissue fibrosis identified by delayed enhancement MRI and atrial fibrillation catheter ablation: the DECAAF study. *JAMA*. 2014;311:498–506. doi: 10.1001/jama.2014.3.
15. Knowles BR, Caulfield D, Cooklin M, Rinaldi CA, Gill J, Bostock J, Razavi R, Schaeffter T, Rhode KS. 3-D visualization of acute RF ablation lesions using MRI for the simultaneous determination of the patterns of necrosis and edema. *IEEE Trans Biomed Eng*. 2010;57:1467–1475. doi: 10.1109/TBME.2009.2038791.
16. Arujuna A, Karim R, Caulfield D, Knowles B, Rhode K, Schaeffter T, Kato B, Rinaldi CA, Cooklin M, Razavi R, O'Neill MD, Gill J. Acute pulmonary vein isolation is achieved by a combination of reversible and irreversible atrial injury after catheter ablation: evidence from magnetic resonance imaging. *Circ Arrhythm Electrophysiol*. 2012;5:691–700. doi: 10.1161/CIRCEP.111.966523.
17. Harrison JL, Sohns C, Linton NW, Karim R, Williams SE, Rhode KS, Gill J, Cooklin M, Rinaldi CA, Wright M, Schaeffter T, Razavi RS, O'Neill MD. Repeat left atrial catheter ablation: cardiac magnetic resonance prediction of endocardial voltage and gaps in ablation lesion sets. *Circ Arrhythm Electrophysiol*. 2015;8:270–278. doi: 10.1161/CIRCEP.114.002066.
18. Sohns C, Karim R, Harrison J, Arujuna A, Linton N, Sennett R, Lambert H, Leo G, Williams S, Razavi R, Wright M, Schaeffter T, O'Neill M, Rhode K. Quantitative magnetic resonance imaging analysis of the relationship between contact force and left atrial scar formation after catheter ablation of atrial fibrillation. *J Cardiovasc Electrophysiol*. 2014;25:138–145. doi: 10.1111/jce.12298.

19. Karim R, Housden RJ, Balasubramaniam M, Chen Z, Perry D, Uddin A, Al-Beyatti Y, Palkhi E, Acheampong P, Obom S, Hennemuth A, Lu Y, Bai W, Shi W, Gao Y, Peitgen HO, Radau P, Razavi R, Tannenbaum A, Rueckert D, Cates J, Schaeffter T, Peters D, MacLeod R, Rhode K. Evaluation of current algorithms for segmentation of scar tissue from late gadolinium enhancement cardiovascular magnetic resonance of the left atrium: an open-access grand challenge. *J Cardiovasc Magn Reson*. 2013;15:105. doi: 10.1186/1532-429X-15-105.
20. Revishvili AS, Wissner E, Lebedev DS, Lemes C, Deiss S, Metzner A, Kalinin VV, Sopov OV, Labartkava EZ, Kalinin AV, Chmelevsky M, Zubarev SV, Chaykovskaya MK, Tsiklauri MG, Kuck KH. Validation of the mapping accuracy of a novel non-invasive epicardial and endocardial electrophysiology system. *Europace*. 2015;17:1282–1288. doi: 10.1093/europace/euu339.
21. Schroeder W, Martin K, Lorensen B. *The Visualization Toolkit*. 4th ed. New York, NY: Kitware; 2006.
22. Rusinkiewicz S, Levoy M. Efficient variants of the ICP algorithm. Paper presented at: Third International Conference on 3D Digital Imaging and Modeling (3DIM); 2001.
23. Narayan SM, Shivkumar K, Krummen DE, Miller JM, Rappel WJ. Panoramic electrophysiological mapping but not electrogram morphology identifies stable sources for human atrial fibrillation: stable atrial fibrillation rotors and focal sources relate poorly to fractionated electrograms. *Circ Arrhythm Electrophysiol*. 2013;6:58–67. doi: 10.1161/CIRCEP.111.977264.
24. Schade A, Nentwich K, Costello-Boerrigter LC, Halbfass P, Mueller P, Roos M, Barth S, Krug J, Szoelloesi GA, Lapp H, Deneke T. Spatial relationship of focal impulses, rotors and low voltage zones in patients with persistent atrial fibrillation. *J Cardiovasc Electrophysiol*. 2016;27:507–514. doi: 10.1111/jce.12913.
25. Boyle PM, Zahid S, Schwarz EL, Whyte KN, Vigmond EJ, Dubois R, Haissaguerre M, Hocini M, Jais P, Cochet H, Trayanova NA. Local complexity of the fibrosis spatial pattern determines the locations of stable reentrant sources in persistent atrial fibrillation: analysis from patient specific models. Paper presented at: Heart Rhythm Scientific Sessions; May 13–16, 2015; Boston, MA.
26. McDowell KS, Zahid S, Vadakkumpadan F, Blauer J, MacLeod RS, Trayanova NA. Virtual electrophysiological study of atrial fibrillation in fibrotic remodeling. *PLoS One*. 2015;10:e0117110. doi: 10.1371/journal.pone.0117110.
27. Chrispin J, Gucuk Ipek E, Zahid S, Prakosa A, Habibi M, Spragg D, Marine JE, Ashikaga H, Rickard J, Trayanova NA, Zimmerman SL, Zipunnikov V, Berger RD, Calkins H, Nazarian S. Lack of regional association between atrial late gadolinium enhancement on cardiac magnetic resonance and atrial fibrillation rotors. *Heart Rhythm*. 2016;13:654–660. doi: 10.1016/j.hrthm.2015.11.011.
28. Spragg DD, Khurram I, Zimmerman SL, Yarmohammadi H, Barcelon B, Needleman M, Edwards D, Marine JE, Calkins H, Nazarian S. Initial experience with magnetic resonance imaging of atrial scar and co-registration with electroanatomic voltage mapping during atrial fibrillation: success and limitations. *Heart Rhythm*. 2012;9:2003–2009. doi: 10.1016/j.hrthm.2012.08.039.
29. Akoum N, Morris A, Perry D, Cates J, Burgon N, Kholmovski E, MacLeod R, Marrouche N. Substrate modification is a better predictor of catheter ablation success in atrial fibrillation than pulmonary vein isolation: an LGE-MRI Study. *Clin Med Insights Cardiol*. 2015;9:25–31. doi: 10.4137/CMC.S22100.
30. Narayan SM, Baykaner T, Clopton P, Schricker A, Lalani GG, Krummen DE, Shivkumar K, Miller JM. Ablation of rotor and focal sources reduces late recurrence of atrial fibrillation compared with trigger ablation alone: extended follow-up of the CONFIRM trial (Conventional Ablation for Atrial Fibrillation With or Without Focal Impulse and Rotor Modulation). *J Am Coll Cardiol*. 2014;63:1761–1768. doi: 10.1016/j.jacc.2014.02.543.
31. Buch E, Share M, Tung R, Benharash P, Sharma P, Koneru J, Mandapati R, Ellenbogen KA, Shivkumar K. Long-term clinical outcomes of focal impulse and rotor modulation for treatment of atrial fibrillation: a multicenter experience. *Heart Rhythm*. 2016;13:636–641. doi: 10.1016/j.hrthm.2015.10.031.
32. Mohanty S, Gianni C, Mohanty P, Halbfass P, Metz T, Trivedi C, Deneke T, Tomassoni G, Bai B, Al-Ahmad A, Bailey S, Burkhardt JD, Gallinghouse GJ, Horton R, Hranitzky PM, Sanchez GE, Biase LD, Natale A. Impact of rotor ablation in non-paroxysmal AF patients: results from a randomized trial (OASIS). *J Am Coll Cardiol*. 2016;68:274–282.
33. Akoum N, Wilber D, Hindricks G, Jais P, Cates J, Marchlinski F, Kholmovski E, Burgon N, Hu N, Mont L, Deneke T, Duytschaever M, Neumann T, Mansour M, Mahnkopf C, Hutchinson M, Herweg B, Daoud E, Wissner E, Brachmann J, Marrouche NF. MRI assessment of ablation-induced scarring in atrial fibrillation: analysis from the DECAAF Study. *J Cardiovasc Electrophysiol*. 2015;26:473–480. doi: 10.1111/jce.12650.